Phase diagram of a frustrated Heisenberg antiferromagnet on the honeycomb lattice: The J_1-J_2-J_3 model

P. H. Y. Li and R. F. Bishop
School of Physics and Astronomy, Schuster Building, The University of Manchester, Manchester M13 9PL, United Kingdom

D. J. J. Farnell
Division of Mathematics, Faculty of Advanced Technology, University of Glamorgan, Pontypridd CF37 1DL, Wales, United Kingdom

C. E. Campbell
School of Physics and Astronomy, University of Minnesota, 116 Church Street SE, Minneapolis, Minnesota 55455, USA

(Received 11 April 2012; revised manuscript received 27 September 2012; published 9 October 2012)

We use the coupled-cluster method in high orders of approximation to make a comprehensive study of the ground-state (GS) phase diagram of the spin-1/2 J_1-J_2-J_3 model on a two-dimensional honeycomb lattice with antiferromagnetic (AFM) interactions up to third-nearest neighbors. Results are presented for the GS energy and the average local onsite magnetization. With the nearest-neighbor coupling strength $J_1 \equiv 1$, we find four magnetically ordered phases in the parameter window $J_2, J_3 \in [0,1]$, namely, the Néel, striped, and Néel-II collinear AFM phases, plus a spiral phase. The Néel-II phase appears as a stable GS phase in the classical version of the model only for values $J_3 < 0$. Each of these four ordered phases shares a boundary with a disordered quantum paramagnetic (QP) phase, and at several widely separated points on the phase boundaries the QP phase has an infinite susceptibility to plaquette valence-bond crystalline order. We identify all of the phase boundaries with good precision in the parameter window studied, and we find three tricritical quantum critical points therein at (a) $(J_2^{c1}, J_3^{c1}) = (0.51 \pm 0.01, 0.69 \pm 0.01)$ between the Néel, striped, and QP phases; (b) $(J_2^{c2}, J_3^{c2}) = (0.65 \pm 0.02, 0.55 \pm 0.01)$ between the striped, spiral, and QP phases; and (c) $(J_2^{c3}, J_3^{c3}) = (0.69 \pm 0.01, 0.12 \pm 0.01)$ between the spiral, Néel-II, and QP phases.

DOI: 10.1103/PhysRevB.86.144404 PACS number(s): 75.10.Jm, 75.50.Ee, 03.65.Ca

I. INTRODUCTION

A combination of strong quantum fluctuations and strong frustration in a spin system provides an ideal scenario for the emergence of such novel quantum ground-state (GS) phases as the quantum spin-liquid (QSL) and other quantum paramagnetic (QP) phases, which do not possess the magnetic long-range order (LRO) that typifies the classical GS phases of the corresponding models taken in the limit $s \to \infty$ of the spin quantum number s of the lattice spins. Quantum fluctuations tend to be largest for the smallest values of s, for lower dimensionality D, and for the smallest coordination number z of the lattice. Thus, for spin-1/2 models, the honeycomb lattice plays a special role since its coordination number ($z = 3$) is the lowest possible for $D = 2$. Frustration is easily incorporated by the inclusion of competing next-nearest-neighbor (NNN) and possibly also next-next-nearest-neighbor (NNNN) bonds. For these reasons, such spin-1/2 frustrated Heisenberg models on the honeycomb lattice have engendered huge theoretical interest.[1–15]

Interest in the honeycomb lattice has been given further impetus by the discovery of a QSL phase in the exactly solvable Kitaev model,[16] in which the spin-1/2 particles are sited on a honeycomb lattice. Interest has also emanated from the synthesis of graphene monolayers[17] and other magnetic materials with a honeycomb structure. For example, it is likely that Hubbard-type models on the honeycomb lattice describe many of the physical properties of graphene. It is interesting to note too the clear evidence of Meng *et al.*[18] that quantum fluctuations are strong enough to trigger an insulating QSL phase between the nonmagnetic metallic phase and the antiferromagnetic (AFM) Mott insulator for the Hubbard model on the honeycomb lattice at moderate values of the Coulomb repulsion U. This latter Mott insulator phase corresponds in the limit $U \to \infty$ to the pure Heisenberg antiferromagnet (HAFM) on the bipartite honeycomb lattice, the GS phase of which exhibits Néel LRO. However, higher-order terms in the t/U expansion of the Hubbard model (where t is the Hubbard hopping term strength parameter) lead to frustrating exchange couplings in the corresponding spin-lattice limiting model (and see, e.g., Ref. 19), in which the HAFM with NN exchange couplings is the leading term in the large-U expansion.

The unexpected result of Meng *et al.*,[18] together with other related work,[19–21] has excited much interest in understanding the physics of frustrated quantum magnets on the honeycomb lattice. A growing consensus is emerging[2,4,7,9,10,12] that frustrated spin-1/2 HAFMs on the honeycomb lattice exhibit a frustration-induced QP phase. Recent experiments[22] on the layered compound $Bi_3Mn_4O_{12}(NO_3)$ (BMNO) at temperatures below its Curie-Weiss temperature reveal QSL-like behavior. In BMNO, the Mn^{4+} ions are situated on the sites of (weakly coupled) honeycomb lattices, although they have spin quantum number $s = \frac{3}{2}$. The successful substitution of the $s = \frac{3}{2}$ Mn^{4+} ions in BMNO by V^{4+} ions could lead to a corresponding experimental realization of a spin-1/2 HAFM on the honeycomb lattice.

Other realizations of quantum HAFMs which exhibit the honeycomb structure include magnetic compounds such as $InNa_3Cu_2SbO_6$ (Ref. 23) and $InCu_{2/3}V_{1/3}O_3$ (Ref. 24). In both of these materials, the Cu^{2+} ions in the copper oxide

layers form a spin-1/2 HAFM on a (distorted) honeycomb lattice. Other similar honeycomb materials include the family of compounds $BaM_2(XO_4)_2$ (M = Co, Ni; X = P, As),[25] in which the magnetic ions M are disposed in weakly coupled layers where they are situated on the sites of a honeycomb lattice. The Co ions have spins $s = \frac{1}{2}$ and the Ni ions have spins $s = 1$. Recent calculations[26] of the material β-$Cu_2V_2O_7$ have demonstrated that its properties can also be described in terms of a spin-1/2 model on an (anisotropic) honeycomb lattice.

The aim of this work is to investigate the phase diagram of the full spin-1/2 J_1-J_2-J_3 model on the honeycomb lattice in the case where all of the NN, NNN, and NNNN bonds are AFM, and we limit the parameter space window to $J_2/J_1, J_3/J_1 \in [0,1]$.

II. HONEYCOMB MODEL

The spin-1/2 J_1-J_2-J_3 model on the honeycomb lattice, or special cases of it (e.g., when $J_3 = J_2$ or $J_3 = 0$), have been intensively studied by many authors (see, e.g., Refs. 1–15 and references cited therein). The Hamiltonian of the model is

$$H = J_1 \sum_{\langle i,j \rangle} \mathbf{s}_i \cdot \mathbf{s}_j + J_2 \sum_{\langle\langle i,k \rangle\rangle} \mathbf{s}_i \cdot \mathbf{s}_k + J_3 \sum_{\langle\langle\langle i,l \rangle\rangle\rangle} \mathbf{s}_i \cdot \mathbf{s}_l \,, \quad (1)$$

where i runs over all lattice sites, and where j, k, and l run over all NN sites, all NNN sites, and all NNNN sites to i, respectively, counting each bond once and once only. Each site i of the lattice carries a spin-s particle represented by an SU(2) spin operator $\mathbf{s}_i = (s_i^x, s_i^y, s_i^z)$. We restrict ourselves here to the case $s = \frac{1}{2}$. The lattice and the exchange bonds are illustrated in Fig. 1.

Before discussing the $s = \frac{1}{2}$ version of the model, it is useful to consider first the classical limit (i.e., $s \to \infty$). The classical version of the model has six GS phases in the case where $J_1 > 0$ and where J_2 and J_3 are arbitrary (i.e., can take either sign).[1,2] Generically, they represent spiral configurations which may be characterized by an ordering wave vector $\mathbf{Q}$, in terms of which the classical spin located at cell $\mathbf{R}$ of the triangular Bravais lattice on either of the two triangular sublattices α (=1,2) of the honeycomb lattice is given by

$$\mathbf{s}_{\mathbf{R},\alpha} = s[\cos(\mathbf{Q}\cdot\mathbf{R} + \theta_\alpha)\mathbf{u} + \sin(\mathbf{Q}\cdot\mathbf{R} + \theta_\alpha)\mathbf{v}] \,, \quad (2)$$

where $\mathbf{u}$ and $\mathbf{v}$ are two orthogonal unit vectors that define the plane of the spins. Clearly, we may choose θ_α to be zero on one of the two sublattices and θ on the other.

The six phases comprise three collinear AFM phases with different ordering wave vectors $\mathbf{Q}$, the FM phase (in which $\mathbf{Q} = 0$ and $\theta = 0$), plus two different helical phases (and see, e.g., Fig. 2 of Ref. 2). The three AFM phases are the Néel phase (in which $\mathbf{Q} = 0$ and $\theta = \pi$), the striped phase, and the Néel-II phase, as shown in Figs. 1(a), 1(b), and 1(d), respectively. (Note that what we refer to as the Néel-II phase here was previously denoted as the anti-Néel phase in earlier papers.[14,15])

Although at zero temperature ($T = 0$) there exists an infinite family of noncoplanar states degenerate in energy with respect to each of the striped and Néel-II states, both thermal and quantum fluctuations[2] favor the collinear configurations. When $J_3 > 0$, the spiral state shown in Fig. 1(c) is the stable classical GS phase in some region of the parameter space. The classical GS energy for this spiral state is minimized when the pitch angle takes the value $\phi = \cos^{-1}[\frac{1}{4}(J_1 - 2J_2)/(J_2 - J_3)]$.

When $\phi \to 0$, this spiral state simply becomes the collinear Néel state. The phase transition between this spiral state and the Néel state is a continuous one and the corresponding phase boundary is given by the equation $y = \frac{3}{2}x - \frac{1}{4}$, for $\frac{1}{6} < x < \frac{1}{2}$, where $y \equiv J_3/J_1$ and $x \equiv J_2/J_1$. Similarly, when $\phi \to \pi$, this spiral state becomes the collinear striped state. These two states undergo a continuous phase transition along their common phase boundary $y = \frac{1}{2}x + \frac{1}{4}$, for $x > \frac{1}{2}$. Furthermore, there is a first-order phase transition between the collinear Néel and striped states along the boundary line $x = \frac{1}{2}$, for $y > \frac{1}{2}$. These three phases (Néel, striped, and spiral) meet at the tricritical point $(x,y) = (\frac{1}{2}, \frac{1}{2})$. We note too that as $x \to \infty$ (for a fixed finite value of y), the spiral pitch angle $\phi \to \frac{2}{3}\pi$. Thus, in this limiting case the classical model simply becomes two HAFMs on weakly connected interpenetrating triangular lattices, with the classical triangular-lattice ordering of NN spins oriented at an angle $\frac{2}{3}\pi$ to each other on each sublattice.

When $y > 0$ (and $J_1 > 0$), the above three states are the only classical GS phases. When $y < 0$, the Néel state persists in a region bounded by the same boundary line $y = \frac{3}{2}x - \frac{1}{4}$, for $-\frac{1}{2} < x < \frac{1}{6}$, on which it continuously meets a second spiral state, and by the boundary line $y = -1$, for $x < -\frac{1}{2}$, at which it undergoes a first-order transition to the FM state, which is the stable GS phase in the region $x < -\frac{1}{2}$ and $y < -1$. Another collinear AFM state, the Néel-II state shown in Fig. 1(d), becomes the stable GS phase in the region $x > \frac{1}{2}$, for $y < \frac{1}{2}\{x - [x^2 + 2(x - \frac{1}{2})^2]^{1/2}\}$. On the boundary, it undergoes a first-order transition to the spiral state in Fig. 1(c).

Finally, for $\frac{1}{6} < x < \frac{1}{2}$, the spiral state in Fig. 1(c) meets a second spiral GS phase, which is characterized by two pitch

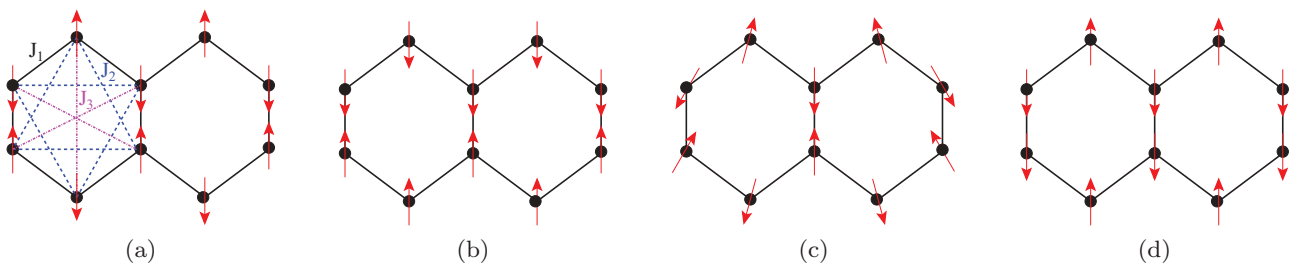

FIG. 1. (Color online) The J_1-J_2-J_3 honeycomb model with $J_1 \equiv 1$; $J_2 > 0$; $J_3 > 0$, showing the (a) Néel, (b) striped, (c) spiral, and (d) Néel-II states. The spins on lattice sites (solid dots) are represented by the (red) arrows.

angles, on the boundary line $y = 0$, along which there is a first-order transition between the two spiral states. Both pitch angles of this second spiral phase smoothly approach the value zero along the above boundary with the Néel state, and the value π along a second boundary curve that joins the points $(x,y) = (-\frac{1}{2},-1)$ and $(\frac{1}{2},0)$, on which it meets the Néel-II state. Both transitions are continuous. This second spiral phase meets the three collinear states Néel, Néel-II, and FM at the tetracritical point $(x,y) = (-\frac{1}{2},-1)$.

In this paper we study the spin-1/2 model of Eq. (1) on the honeycomb lattice in the case where all of the bonds are antiferromagnetic in nature. Henceforth, we set $J_1 \equiv 1$ to set the overall energy scale, and we work here within the parameter space window $J_2, J_3 \in [0,1]$.

III. CCM FORMALISM

The coupled-cluster method (CCM) is a widely used microscopic many-body technique. It efficiently and accurately handles a wide variety of highly frustrated quantum magnets.[8,13–15,27–35] Such frustrated systems are notoriously challenging at the theoretical level. Of the other well-established and widely used techniques, exact diagonalization (ED) methods, which involve the finite-size extrapolation of numerical exact data for finite-lattice systems, are much more challenging for the present honeycomb-lattice model than for comparable square-lattice models, to which they have been very efficiently and accurately applied (see, e.g., Refs. 34, 36, and 37). The reasons include the facts that for the honeycomb lattice the unit cell now contains two sites, and that there exist relatively fewer finite-sized lattices (than in the square-lattice case) that are small enough for ED methods to be used but which also contain the full point-group symmetry.[2]

The CCM is a size-extensive method, in which the limit $N \to \infty$, where N is the number of lattice spins, may automatically be imposed from the outset. The many-body system under study is assumed to have exact ket and bra GS energy eigenvectors $|\Psi\rangle$ and $\langle\tilde{\Psi}|$, respectively, which satisfy the corresponding Schrödinger equations

$$H|\Psi\rangle = E|\Psi\rangle\,, \quad \langle\tilde{\Psi}|H = E\langle\tilde{\Psi}|\,, \tag{3}$$

and which are chosen to have the normalization $\langle\tilde{\Psi}|\Psi\rangle = 1$, i.e., $\langle\tilde{\Psi}| = \langle\Psi|/\sqrt{\langle\Psi|\Psi\rangle}$. The quantum correlations present in the exact ground state are expressed systematically in the CCM with respect to some suitable normalized model (or reference) state $|\Phi\rangle$.[27] In this study, we choose various classical model states as our CCM model states, namely, (a) the Néel, (b) the striped, (c) the spiral, and (d) the Néel-II states shown in Fig. 1.

The CCM parametrizations of the exact ket and bra GS wave functions are

$$|\Psi\rangle = e^{S}|\Phi\rangle\,, \quad \langle\tilde{\Psi}| = \langle\Phi|\tilde{S}e^{-S}\,, \tag{4}$$

where the CCM correlation operators S and $\tilde{S}$ are themselves expressed as generalized multiconfigurational creation and destruction operators, respectively,

$$S = \sum_i \mathcal{S}_I C_I^+, \quad \tilde{S}_I = 1 + \sum_i \tilde{\mathcal{S}}_i C_I^-, \quad \forall I \neq 0. \tag{5}$$

They satisfy the normalization relations $\langle\tilde{\Psi}|\Psi\rangle = \langle\Phi|\Psi\rangle = \langle\Phi|\Phi\rangle \equiv 1$. The operators $C_I^+ \equiv (C_I^-)^\dagger$, with $C_0^\dagger \equiv 1$, have the property that $\langle\Phi|C_I^+ = 0 = C_I^-|\Phi\rangle = 0\ ;\ \forall I \neq 0$. The correlation coefficients $(\mathcal{S}_I,\ \tilde{\mathcal{S}}_I)$ are determined by requiring the energy expectation value $\bar{H} \equiv \langle\tilde{\Psi}|H|\Psi\rangle$ to be a minimum with respect to each of them. This results in the coupled sets of equations $\langle\Phi|C_I^- e^{-S}He^{S}|\Phi\rangle = 0$ and $\langle\Phi|\tilde{S}(e^{-S}He^{S} - E)C_I^+|\Phi\rangle = 0;\ \forall I \neq 0$, which we solve for the correlation coefficients $(\mathcal{S}_I,\ \tilde{\mathcal{S}}_I)$ once the specific truncation scheme is specified.

In order to treat each lattice site in the spin system on an equal basis, it is extremely convenient to rotate the local spin axes on each site in such a way that all the spins of each CCM reference state used point along the negative z direction. The multispin creation operators may then be written as linear sums of products of the individual spin-raising operators $s_k^+ \equiv s_k^x + is_k^y$, i.e., $C_I^+ \equiv s_{k_1}^+ s_{k_2}^+ \ldots s_{k_n}^+$. After calculation of the correlation coefficients $(\mathcal{S}_I,\ \tilde{\mathcal{S}}_I)$, we can then calculate the GS energy using $E = \langle\Phi|e^{-S}He^{S}|\Phi\rangle$, and the magnetic order parameter, which is defined to be the average local onsite magnetization $M \equiv -\frac{1}{N}\langle\tilde{\Psi}|\sum_{i=1}^{N} s_i^z|\Psi\rangle$, with respect to the local rotated-spin coordinates described above.

For spin-1/2 systems, we use the well-established localized lattice-animal-based subsystem (LSUBm) truncation scheme where we keep at a given truncation level specified by the index m only all of those multispin configurations which may be defined over all possible lattice animals (or polyominoes) of size m on the lattice. A lattice animal (or polyomino) of size m is defined as a set of m contiguous sites in the usual graph-theoretic sense where every site is adjacent (in the nearest-neighbor sense) to at least one other site.

Table I shows the number N_f of fundamental configurations that are inequivalent after all space- and point-group symmetries of both the Hamiltonian and the model state have been taken into account, for each of the Néel, striped, spiral, and Néel-II model states. The parameter N_f increases rapidly with the truncation index m. We use massively parallel computing to derive and solve the corresponding coupled sets of CCM bra and ket state equations for high-order LSUBm approximations.[38]

TABLE I. Number of fundamental configurations N_f for the spin-1/2 J_1-J_2-J_3 model ($J_1 = 1$) on the honeycomb lattice, using the Néel, striped, Néel-II, and spiral states.

	N_f			
Method	Néel	Striped	Néel-II	Spiral
LSUB4	5	9	9	66
LSUB6	40	113	85	1080
LSUB8	427	1750	1101	18986
LSUB10	6237	28805	17207	347287

As a last step, we need to extrapolate the LSUBm data to reach results in the exact $m \to \infty$ limit. For the GS energy per spin E/N, a well-established and very accurate extrapolation ansatz (see, e.g., Refs. 28–35) is

$$E(m)/N = a_0 + a_1 m^{-2} + a_2 m^{-4}, \tag{6}$$

whereas for the magnetic order parameter M for systems with a considerable degree of frustration, such as is the case for the present model, we use (see, e.g., Refs. 8, 13–15, 30–32, 34,

and 35)

$$M(m) = c_0 + c_1 m^{-1/2} + c_2 m^{-3/2}. \quad (7)$$

When we have only three data points to fit to an extrapolation formula, a two-term extrapolation fit can easily be preferable in practice to a three-term fit. In such cases we sometimes use the alternative simpler forms

$$E(m)/N = b_0 + b_1 m^{-2} \quad (8)$$

and

$$M(m) = d_0 + d_1 m^{-1/2}, \quad (9)$$

instead of their counterparts in Eqs. (6) and (7).

IV. PREVIEW OF THE PHASE DIAGRAM

Before discussing our results in detail, we first summarize our main findings by showing in Fig. 2 the phase diagram in the case where all the bonds are antiferromagnetic in nature (i.e., $J_n > 0, n = 1,2,3$). Furthermore, we set $J_1 \equiv 1$ and restrict ourselves to the window $0 \leqslant J_m \leqslant 1$, $m = 2,3$. Henceforth, we denote $x \equiv J_2/J_1$, $y \equiv J_3/J_2$. The actual phase boundaries are determined from a variety of information that emerges from our CCM calculations, as we now describe briefly and with further details given in Sec. V.

We have previously studied this model for the two special cases with $J_3 = J_2$ in Ref. 8, and with $J_3 = 0$ in Ref. 14, and the corresponding CCM results from those papers are included in Fig. 2. First, along the line $J_3 = J_2$ (i.e., when $y = x \equiv \kappa$), we found[8] that the system has quasiclassical AFM Néel order for $\kappa < \kappa_{c_1} \approx 0.47$, quasiclassical AFM striped order for $\kappa > \kappa_{c_2} \approx 0.60$, and a quantum paramagnetic phase separating the Néel and striped phases for $\kappa_{c_1} < \kappa < \kappa_{c_2}$. By studying the susceptibility of the Néel and striped states to hexagonal plaquette valence-bond crystalline (PVBC) ordering, we found that the most likely scenario was that the intervening state had PVBC order over the entire range $\kappa_{c_1} < \kappa < \kappa_{c_2}$. The transition at $\kappa = \kappa_{c_2}$ between the PVBC and striped GS phases was seen to be of first-order type, while that at $\kappa = \kappa_{c_1}$ between the Néel and PVBC GS phases appeared to be a continuous one. Since the Néel and PVBC phases break different symmetries, our results favored the transition point between them at $\kappa = \kappa_{c_1}$ to be a deconfined quantum critical point (QCP). The QCPs at $y = x = \kappa_{c_1}$ and at $y = x = \kappa_{c_2}$ are clearly shown in Fig. 2 with the larger (red) times (×) and the larger (green) plus (+) symbols, respectively.

Second, in a separate study along the line $y = 0$, we found[14] that the system has the quasiclassical Néel state as its GS phase for $x < x_{c_1} \approx 0.21$, the quasiclassical Néel-II state as its GS phase for $x > x_{c_2} \approx 0.39$, and again a QP phase separating the Néel and Néel-II phases for $x_{c_1} < x < x_{c_2}$. Similar CCM calculations of the susceptibility of the Néel and Néel-II phases to PVBC order led again to the conclusion that the transition between the PVBC and Néel-II phases was of first-order type, while the likely scenario for the transition between the Néel and PVBC phases is again that it is of the continuous deconfined type. Nevertheless, due to the difficulty in determining the lower critical value of x at which PVBC order is established as accurately as we determined the value $x = x_{c_1}$ at which Néel order is destabilized, we could not exclude a second scenario in which the transition between the Néel and PVBC phases proceeds via an intervening phase (possibly even of an exotic QSL variety) in the very narrow window $0.21 \lesssim x \lesssim 0.24$. Again, the QCPs at $(x,y) = (x_{c_1},0)$ and $(x_{c_2},0)$ are clearly shown in Fig. 2.

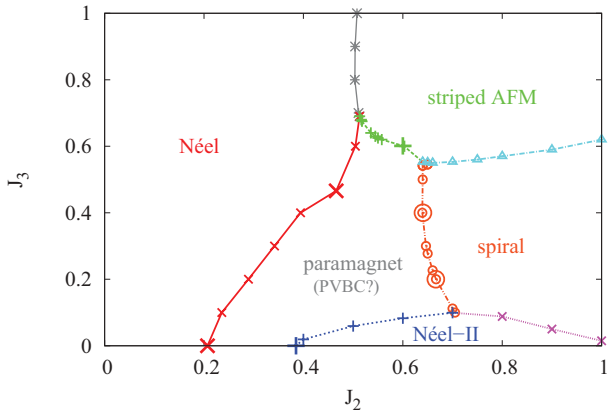

FIG. 2. (Color online) Phase diagram of the spin-1/2 J_1-J_2-J_3 model on the honeycomb lattice (with $J_1 \equiv 1$) in the parameter window $J_2, J_3 \in [0,1]$. The five regions correspond to four quasiclassical phases with (a) AFM Néel order as in Fig. 1(a), (b) collinear AFM striped order as in Fig. 1(b), (c) spiral order as in Fig. 1(c), (d) AFM Néel-II order as in Fig. 1(d), plus (e) a magnetically disordered, or quantum paramagnetic (QP), phase that exhibits plaquette valence-bond crystalline (PVBC) order on at least part of the boundary region (and see the following). The first-order phase transition boundary between the Néel and striped phases, marked by the (gray) convolution (eight-pointed star ∗) symbols is found from points at which the curves for the magnetic order parameter M of the two phases cross; the first-order phase transition boundary between the striped and QP phases, marked by (green) plus (+) symbols, is found from points at which $M \to 0$ for the striped phase; the first-order phase-transition boundary between the striped and spiral phases, marked by (cyan) open triangle (△) symbols, is found from points at which the curves for the magnetic order parameter M of the two phases cross; the phase-transition boundary between the spiral and QP phases, marked by (orange) open circle (◯) symbols (of two sizes, see main text in Sec. V B), is found from points at which $M \to 0$ for the spiral phase; the first-order phase-transition boundary between the spiral and Néel-II states, marked by (magenta) times (×) symbols, is found from points at which the curves for the magnetic order parameter M of the two phases cross; the phase-transition boundary between the Néel-II and QP phases, marked by (blue) plus (+) symbols, is found from points at which $M \to 0$ for the Néel-II phase; and the phase-transition boundary between the Néel and QP states, marked by (red) times (×) symbols, which is probably of continuous (second-order, and possibly of a deconfined) nature, is found from points at which $M \to 0$ for the Néel phase. Points marked by the larger (red) times (×) and (green and blue) plus (+) symbols are found to be infinitely susceptible to PVBC order, and hence the QP state at these points is PVBC in nature.

We also showed previously,[14] by a comparison of the GS energies of the spiral and Néel-II phases, that the spiral phases that are present classically (i.e., for the case where the spin quantum number $s \to \infty$) in the case $y = 0$ for all values $x > \frac{1}{6}$ are absent for all values $x \lesssim 1$. The actual phase boundary between the spiral and Néel-II phases shown in

Fig. 2 is now calculated in this paper, as described in the following.

Based on our previous findings for the GS phases of these two special cases when (a) $J_3 = J_2$ and (b) $J_3 = 0$, we have performed a series of CCM calculations based on the Néel, striped, Néel-II, and spiral states as model states, for various cuts in the phase diagram at constant values of either J_3 or J_2. For example, the phase boundary between the Néel and the striped phases is obtained, as explained more fully in Sec. V A, from our extrapolated ($m \to \infty$) LSUBm results for the order parameter M (namely, the average onsite magnetization) of the two phases, for a variety of constant J_3 cuts. We find that for values of $y \equiv J_3/J_1 \gtrsim 0.69$, the two magnetization curves meet at a (positive) nonzero value, indicative of a direct first-order transition between the states.

For $y \approx 0.69$, the two curves become zero at precisely the same point $x \approx 0.51$. Conversely, when $y \lesssim 0.69$, the order parameters of both the Néel and striped phases become zero at respective critical values of x before the curves cross (when solutions exist for both phases), indicating the emergence of a new phase separating them. The corresponding points where the magnetic order parameters for Néel order and striped order vanish are shown in Fig. 2 by (red) times ($\times$) and (green) plus ($+$) symbols, respectively. By continuity with our earlier results[8] along the line $y = x$, we tentatively identify the intervening phase as the PVBC state. The tricritical QCP between the Néel, striped, and PVBC phases is thus identified as being at $(x,y) \approx (0.51,0.69)$. For values of $y \lesssim 0.55$, no solution for the striped phase exists with $M > 0$ for any value of x, giving first indications of a new phase boundary between the striped state and another phase that we identify as a spiral phase.

By comparing the order parameters for the striped and spiral phases at various constant J_2 cuts, we find that for values of $x \gtrsim 0.66$, the two curves meet at a (positive) nonzero value, again indicative of a direct transition between the states. These points are shown in Fig. 2 as (cyan) open triangle ($\triangle$) symbols. For $x \approx 0.66$, the two curves become zero at the same point $y \approx 0.55$. For values $x \lesssim 0.66$, the order parameters of both the striped and spiral phases become zero at respective critical values of y before the curves cross. Again, this indicates a phase separating these phases for values of $x \lesssim 0.66$ (down to a lower value of $x \approx 0.635$ below which the spiral phase ceases to exist for any value of y), which we again identify tentatively as the PVBC phase.

In that very narrow window $0.635 \lesssim x \lesssim 0.66$, which is almost certainly an artifice of our approximations, we denote in Fig. 2 the points where the magnetic order parameter vanishes ($M \to 0$) for the striped and spiral states by (cyan) open triangle ($\triangle$) and (orange) open circle ($\bigcirc$) symbols, respectively. We argue in Sec. V C that these results are consistent with the existence of a second tricritical QCP at $(x,y) \approx (0.65,0.55)$ between the striped, spiral, and (tentatively) PVBC phases. The remainder of the phase boundary between the spiral and PVBC states is similarly identified by the vanishing of the magnetic order parameter of the spiral phase, and these points are again shown in Fig. 2 as (orange) open circle ($\bigcirc$) symbols.

Finally, by comparing the energies of the Néel-II and spiral phases, we find that for all values of the parameter $J_2 \leqslant 1$ where the spiral phase exists, the Néel-II phase actually has a lower energy for values of the parameter J_3 below a certain critical value, which itself depends on J_2. Similarly, by comparing the order parameters of these two phases at various constant J_2 cuts, we find that for values of $x \gtrsim 0.69$, the two curves meet at a (positive) nonzero value, indicative once more of a direct phase transition between the Néel-II and spiral phases. These points are shown in the phase diagram of Fig. 2 by (magenta) times ($\times$) symbols.

For $x \approx 0.69$, the two curves become zero at the same point $y \approx 0.12$. Conversely, for $x \lesssim 0.69$, the order parameters of the Néel-II and spiral phases both become zero at respective critical values of y before the curves cross. This is again indicative of a phase separating the Néel-II and spiral phases for $x \lesssim 0.69$ (down to the lower value of $x \approx 0.635$ below which the spiral phase ceases to exist for any value of y), as noted above. This intermediate phase is again tentatively identified as having PVBC order. In this way we identify a third tricritical QCP at $(x,y) \approx (0.69,0.12)$ between the spiral, Néel-II, and (tentatively) PVBC phases. Remaining points on the boundary between the Néel-II and PVBC phases are then identified by where the magnetic order parameter of the Néel-II phase vanishes, shown by (blue) plus ($+$) symbols on the the phase diagram of Fig. 2.

In Sec. V we now describe in more detail how the various points in the phase diagram of Fig. 2 are obtained.

V. RESULTS

In this section we present and discuss our CCM results for the spin-1/2 J_1-J_2-J_3 HAFM on the honeycomb lattice.

A. Néel versus striped phases

Figure 3 shows the extrapolated ($m \to \infty$) CCM LSUBm values for the GS energy per spin for the Néel and striped states as functions of J_2 for various fixed values of J_3. The energy curves cross for all values of the parameter $J_3 \gtrsim 0.68$, but not for values $J_3 \lesssim 0.68$. This gives us a first indication of the emergence of an intermediate phase between the Néel and

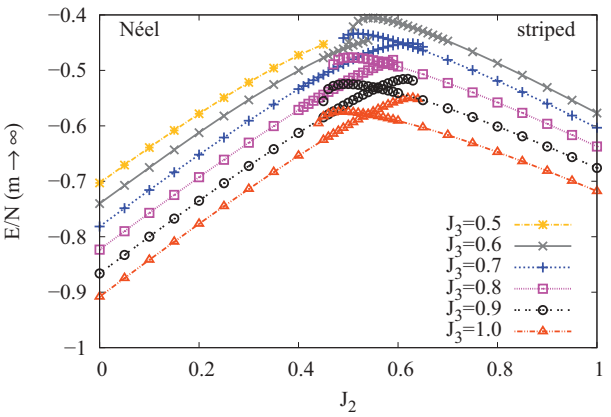

FIG. 3. (Color online) Extrapolated CCM LSUB∞ results for the GS energy per spin E/N as a function of J_2, for various fixed values of J_3 in the range $0.5 \leqslant J_3 \leqslant 1.0$, for the Néel and the striped states. The extrapolated LSUBm ($m \to \infty$) results are based on the scheme of Eq. (6) and the calculated results with $m = \{6,8,10\}$.

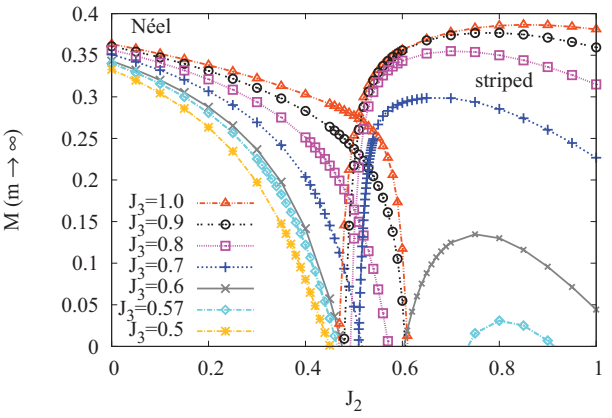

FIG. 4. (Color online) Extrapolated CCM LSUB∞ results for the GS magnetic order parameter M as a function of J_2, for various fixed values of J_3 in the range $0.5 \leqslant J_3 \leqslant 1.0$, for the Néel and the striped states. The extrapolated LSUBm ($m \to \infty$) results are based on the scheme of Eq. (7) and the calculated results with $m = \{6,8,10\}$.

striped states, over a finite range of values of the J_2 parameter, below some critical value of the J_3 parameter.

The extrapolations become more difficult in the vicinity of this critical point, and consequently the actual values of J_2 at which the curves cross for fixed values of J_3 near the critical value are more uncertain than those at larger values. Furthermore, at the actual energy crossing points very near the critical point, the corresponding values of the magnetic order parameter (i.e., the average onsite magnetization) M for one or both states becomes negative and hence unphysical. Indeed, for the striped state, $M < 0$ for the entire $J_3 = 0.5$ curve, which is why we have not shown it in Fig. 3.

In order to obtain more accurate values of the critical point, we also show in Fig. 4 the curves for the extrapolated order parameters M of the Néel and striped states, corresponding to values of J_3 shown in Fig. 3 for the GS energy per spin E/N. We observe again that the curves intersect when $J_3 \gtrsim 0.69$, and that the corresponding values of (J_2, J_3) are our best estimate for the phase boundary between the Néel and striped states. When $J_3 \lesssim 0.69$, the extrapolated order parameters of both the Néel and striped phases become zero before the curves intersect, revealing an intermediate phase in that regime. Our best value for the corresponding tricritical QCP comes from the data shown in Fig. 4, where it is seen to be at $(J_2^{c_1}, J_3^{c_1}) = (0.51 \pm 0.01, 0.69 \pm 0.01)$, and where the error bars are estimates from a sensitivity analysis of the LSUBm extrapolation scheme.

The extrapolated order parameter M becomes everywhere negative (i.e., for all values of J_2) for the striped state for all values of $J_3 \lesssim 0.55$, as may be seen from data similar to those shown in Fig. 4. This is a clear first indication that the striped state becomes unstable as the GS phase in this regime. From a comparison with the corresponding classical model (i.e., in the limit $s \to \infty$) discussed in Sec. II, we might expect the striped state to yield to the spiral state, at least for sufficiently large values of J_2 in the present $s = \frac{1}{2}$ case. We investigate this further in Sec. V C. It is clearly also expected that the Néel phase will not survive for large enough frustrating values of $J_2 > 0$, and again from a comparison with the classical model we expect that the spiral phase might exist in that case too. Hence, we first make a comparison in Sec. V B of the Néel and spiral phases.

B. Néel versus spiral phases

We start by analyzing the GS energy per spin E/N for the spiral state as a function of the spiral pitch angle ϕ. We choose the angle ϕ, for each point in the phase diagram where the spiral state exists, as the one that minimizes the energy estimate there. Clearly, the minimizing angle depends on the particular LSUBm approximation being used. For example, we show in Fig. 5(a) the GS energy per spin E/N as a function of pitch angle ϕ in the LSUB6 approximation, for various illustrative values of J_2, all with $J_3 = 0.4$.

We note first from Fig. 5(a) that, for various fixed values of J_2, CCM solutions at a given LSUBm level of approximation exist only for certain ranges of the spiral angle ϕ. For example, for $J_2 = 0$, the CCM LSUB6 solutions based on the spiral state exist only for $0 \leqslant \phi \lesssim 0.12\pi$. In this case, where the Néel state

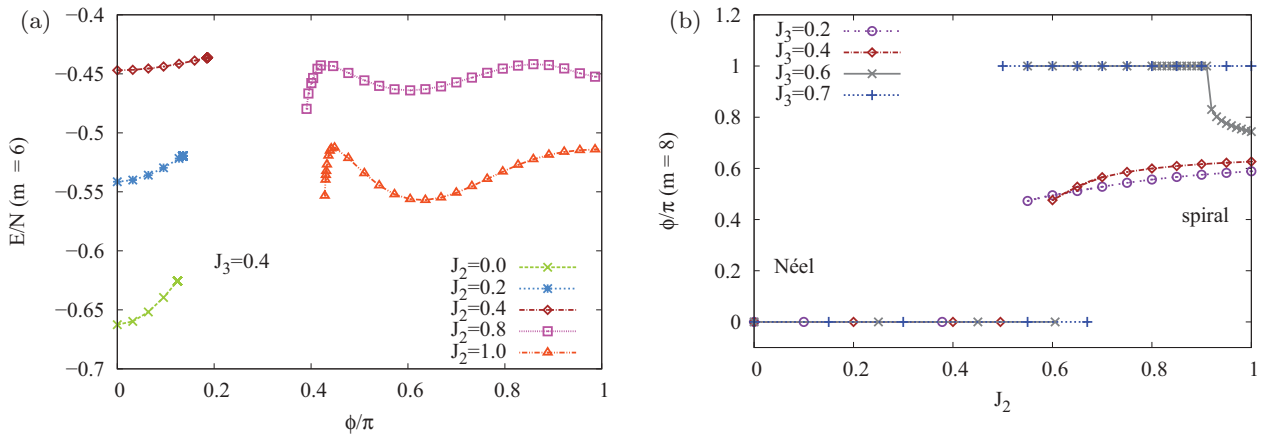

FIG. 5. (Color online) (a) LSUB6 results for the GS energy per spin, using the spiral state as CCM model state, as a function of the spiral pitch angle ϕ, for some illustrative values of J_2 in the range $0 \leqslant J_2 \leqslant 1$ and for a fixed value of $J_3 = 0.4$. (b) The pitch angle $\phi = \phi_{\text{LSUB}m}$ that minimizes the energy $E_{\text{LSUB}m}(\phi)$ of the spiral state. The CCM LSUBm results with $m = 8$ are shown as functions of J_2 for several fixed values of J_3 in the range $0.2 \leqslant J_3 \leqslant 0.7$.

(i.e., where $\phi = 0$) is the stable GS phase that minimizes the energy, if we try to force the system too far away from Néel collinearity, the CCM equations themselves become unstable in the sense that they no longer have a real solution. We note too that as J_2 is increased slowly, the minimum in the energy curve at $\phi = 0$ becomes shallower, so that by the time $J_2 = 0.4$, it has almost disappeared. This is a first indication of the imminent instability of the Néel state as the GS phase if J_2 is increased slightly more.

Similarly, the CCM LSUB6 solutions shown based on the spiral state exist only for $0.43 \lesssim \phi/\pi \leqslant 1$. In this case, a spiral state (i.e., with a value $\phi \neq 0,\pi$) is the stable GS phase that minimizes the energy, and if we now try to force the system too close to the Néel regime, the CCM solution collapses. We also observe from Fig. 5(a) that for the smaller value $J_2 = 0.8$, while the energy curve still shows a global minimum for a noncollinear spiral phase, it has now also developed a secondary minimum at a value $\phi = \pi$ (i.e., that of the collinear striped state), which indicates the proximity of the phase boundary between the spiral and striped states, as we examine more fully in Sec. V C.

Conversely, as J_3 is increased further (for fixed J_2), the spiral minimum becomes more pronounced, and as $J_2 \to \infty$ the pitch angle $\phi \to \frac{2}{3}\pi$. This is as expected since in this limit the model becomes two weakly connected HAFMs on interpenetrating triangular lattices, with the classical ordering of NN spins oriented at angles $\frac{2}{3}\pi$ with respect to one another on each sublattice.

From such data such as shown in Fig. 5(a) we can calculate the angle $\phi = \phi_{\mathrm{LSUB}m}$ that minimizes the energy $E_{\mathrm{LSUB}m}(\phi)$ for given values of the exchange coupling strengths. For example, in Fig. 5(b) we show the angle $\phi = \phi_{\mathrm{LSUB8}}$ from the LSUB8 approximation, as a function of the parameter J_2 for several fixed values of the parameter J_3. There is clear evidence that for values of J_3 below some upper critical value there is no stable spiral solution for any value of $\phi \neq 0$ over a certain range of the parameter J_2, which itself depends on J_3.

Thus, we are led to expect a second tricritical QCP in the (J_2, J_3) plane at $(J_2^{c_2}, J_3^{c_2})$, with $J_3^{c_2} < J_3^{c_1}$, such that (a) for values $J_3 > J_3^{c_1}$ the Néel and striped states meet at a common phase boundary discussed in Sec. V A above, (b) for values $J_3^{c_1} > J_3 > J_3^{c_2}$ there is an intermediate phase between the Néel and striped states, and (c) for values $J_3 < J_3^{c_2}$ there is an intermediate phase between the Néel state and the spiral state with $\phi \neq \pi$. Thus, the QCP at $(J_2^{c_2}, J_3^{c_2})$ is a tricritical point between the Néel, striped, and intermediate phases. From the results discussed in Sec. V A, we now expect that $J_3^{c_2} \approx 0.55$, and we discuss this further below.

Figure 6 shows our results for the GS energy per spin E/N as a function of J_2, for various fixed values of J_3, for the Néel and the spiral states. It clearly illustrates the existence of an intermediate phase between the Néel and the spiral phases (including the striped state as a special case of the latter) for values $J_3 < J_3^{c_1}$.

For the spiral state, the extrapolations are calculated using the LSUBm calculated results with $m = \{4,6,8\}$, rather than with the set $m = \{6,8,10\}$ used for the Néel state. This is partly due to the very high number, $N_f = 347\,287$, of configurations needed for the spiral state at the LSUB10 level of approximation, compared with the corresponding much smaller number, $N_f = 6237$, for the Néel state, as seen from Table I. This difference is compounded by the fact that for the spiral state we need to do LSUBm runs for each point in the phase space as a function of the pitch angle ϕ. This makes LSUBm calculations for the spiral state with $m \geqslant 10$ particularly demanding of computational resources. Nevertheless, we did perform LSUB10 calculations for the spiral state for the special case $J_3 = 0$ in our previous study of the J_1-J_2 model,[14] where we performed separate extrapolations using the LSUBm results with $m = \{6,8,10\}$ and $m = \{4,6,8\}$. We found that both extrapolations were in very good agreement with one another, and hence feel confident that the spiral-state extrapolations for the full J_1-J_2-J_3 model considered here with the limited set $m = \{4,6,8\}$ will be equally robust since it is now prohibitively expensive of computational resource to perform LSUB10 calculations for the spiral state over the whole region of phase space where it is the stable GS phase.

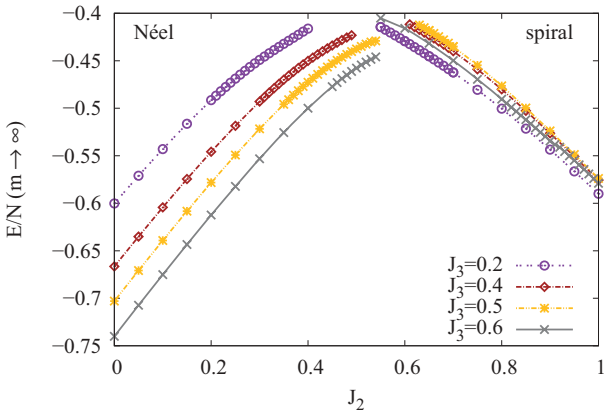

FIG. 6. (Color online) Extrapolated CCM LSUB∞ results for the GS energy per spin E/N as a function of J_2, for various fixed values of J_3 in the range $0.2 \leqslant J_3 \leqslant 0.6$, for the Néel and the spiral states. The extrapolated LSUBm ($m \to \infty$) results are based on the scheme of Eq. (6) and the calculated results with $m = \{6,8,10\}$ for the Néel state, and with $m = \{4,6,8\}$ for the spiral state. For the spiral state, the results use the pitch angle $\phi = \phi_{\mathrm{LSUB}m}$ that minimizes the energy $E = E_{\mathrm{LSUB}m}(\phi)$.

As is usually the case, the CCM LSUBm results for finite m values for a given phase extend beyond the actual physical LSUB∞ boundary for that phase. Thus, the energy curves shown in Fig. 6 for fixed values of J_3 terminate at certain values of J_2, which are determined by the termination points of the highest LSUBm approximations used in the extrapolations, beyond which no real solution exists for the corresponding coupled CCM equations. We note from Fig. 6 that the maxima in the energy curves occur close to these LSUBm termination points for the largest m values employed, which in turn lie close to the physical (LSUB∞) phase-transition points.

We show in Fig. 7 our results for the GS magnetic order parameters M for both the Néel and the spiral states, as functions of J_2, for the same fixed values of J_3 shown in Fig. 6 for the GS energy. As we indicated above, LSUB10 calculations are prohibitively expensive for the spiral state, and hence we need for extrapolation purposes to include the LSUB4 results. When the data set $m = \{4,6,8\}$ is thus

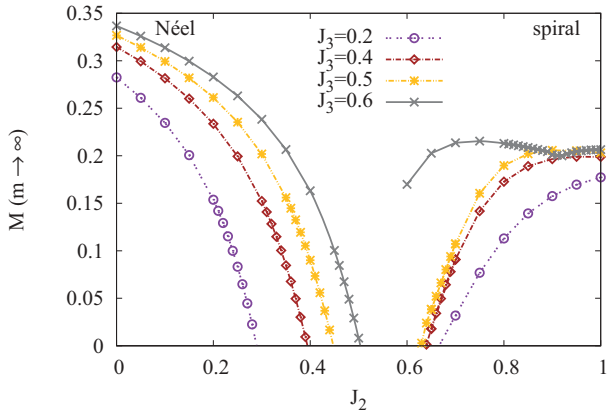

FIG. 7. (Color online) Extrapolated CCM LSUB∞ results for the GS magnetic order parameter M as a function of J_2, for various fixed values of J_3 in the range $0.2 \leqslant J_3 \leqslant 0.6$, for the Néel and the spiral states. The extrapolated LSUBm ($m \to \infty$) results are based on the scheme of Eq. (9) and the calculated results with $m = \{6,8,10\}$ for the Néel state, and with $m = \{4,6,8\}$ for the spiral state. For the spiral state, the results use the pitch angle $\phi = \phi_{\mathrm{LSUB}m}$ that minimizes the energy $E = E_{\mathrm{LSUB}m}(\phi)$.

employed, it is clearly preferable to use the extrapolation scheme of Eq. (9) rather than that of Eq. (7), so as not to give the $m = 4$ result too much weight. As a check we have performed LSUB10 calculations for the two values $J_3 = 0.2, 0.4$, for which we have also made extrapolations using Eq. (9) with $m = \{6,8,10\}$. These are indicated in Fig. 2 by the larger (orange) open circles. We find, gratifyingly, that the two extrapolations agree well with one another at both values $J_3 = 0.2, 0.4$, which gives credence to our results using the data set $m = \{4,6,8\}$ elsewhere for the spiral state.

In our earlier study[14] of this model with $J_3 = 0$, we also computed LSUB12 results for the Néel state and found that the Néel order vanished at a value $J_2 \approx 0.207 \pm 0.003$ when we performed extrapolations including the $m = 12$ point. This point is shown in Fig. 2 by the larger (red) times ($\times$) symbol, although the value obtained with the more limited data set $m = \{6,8,10\}$ used in Fig. 7 is in good agreement with it. Similarly, in our earlier study along the $J_3 = J_2$ line,[8] we also used LSUBm results with $m = \{6,8,10,12\}$ to perform the extrapolations and found that in this case Néel order vanished at a value $J_2 \approx 0.466 \pm 0.005$, and this value is also shown in Fig. 2 by a larger (red) times ($\times$) symbol.

From curves such as those in Fig. 7, we use the points where the extrapolated values of the order parameter M vanish to plot the boundaries of the Néel and spiral phases shown in Fig. 2. As expected from our discussion in Sec. V A, a Néel-ordered phase exists for all values of J_3 up to some critical value of J_2 which marks its phase boundary. For values $J_3 < J_3^{c_1} \approx 0.69 \pm 0.01$, this phase borders a QP phase, whereas for $J_3 > J_3^{c_1}$ it borders the striped state at a first-order phase-transition boundary. Curves such as those in Fig. 7 show clear evidence for an intervening phase between the Néel and spiral phases (with pitch angle $\phi \neq \pi$) everywhere that the spiral phase exists. Instead, the spiral phase meets the striped phase along a common boundary (on which $\phi = \pi$) for all values $J_2 > J_2^{c_2} \gtrsim 0.65$. There is thus a second tricritical point at $(J_2^{c_2}, J_3^{c_2})$, as we discuss more fully in Sec. V C, at which the striped, spiral, and quantum paramagnetic phases meet.

C. Striped versus spiral phases

We recall that classically (i.e., when $s \to \infty$) we have that for a fixed value of $J_2 > \frac{1}{2}$ the GS phase is the striped phase for $J_3 > \frac{1}{2}J_2 + \frac{1}{4}$ and the spiral phase for $J_3 < \frac{1}{2}J_2 + \frac{1}{4}$. There is a continuous phase transition between the two classical states along the boundary line $J_3 = \frac{1}{2}J_2 + \frac{1}{4}, J_2 \geqslant \frac{1}{2}$ on which the spiral pitch angle $\phi = \pi$. Our results for the present $s = \frac{1}{2}$ model, as we shall see in the following, indicate that quantum fluctuations stabilize the collinear order of the striped state to lower values of J_3, for fixed J_2, than the classical limit. Furthermore, the quantum fluctuations also seem to turn the classical second-order transition into a quantum first-order one.

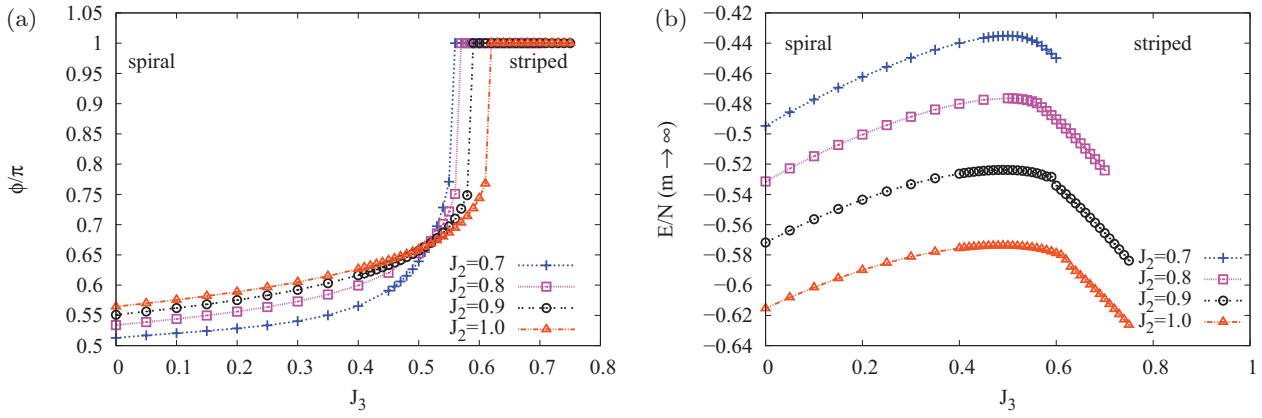

FIG. 8. (Color online) (a) The angle $\phi = \phi_{\mathrm{LSUB}m}$ that minimizes the energy $E_{\mathrm{LSUB}m}(\phi)$. The CCM LSUBm results with $m = 8$ are shown as functions of J_3 for several fixed values of J_2 in the range $0.7 \leqslant J_3 \leqslant 1.0$. Note that $\phi = \pi$ corresponds to the striped state. (b) Extrapolated CCM LSUB∞ results for the GS energy per spin E/N as a function of J_3, for various fixed values of J_2 in the range $0.7 \leqslant J_3 \leqslant 1.0$, for the spiral and the striped states. The extrapolated LSUBm ($m \to \infty$) results are based on the scheme of Eq. (6) and the calculated results with $m = \{4,6,8\}$. For the spiral state, the results use the pitch angle $\phi = \phi_{\mathrm{LSUB}m}$ that minimizes the energy $E = E_{\mathrm{LSUB}m}(\phi)$.

Thus, we show in Fig. 8(a) the angle $\phi = \phi_{\mathrm{LSUB8}}$ that minimizes the energy $E_{\mathrm{LSUB8}}(\phi)$ as a function of J_3, using the spiral state as our CCM model state, for various fixed values of J_2. Similar curves are found for other LSUBm approximations. Unlike in the classical case, where $\phi \to \pi$ continuously at the critical value, there is now a discontinuous jump on the phase boundary. Its origin lies in the double-minimum structure of the corresponding energy curves (for fixed values of J_2 and J_3) as functions of the pitch angle ϕ, comparable to that shown in Fig. 5(a) for the case $J_2 = 0.8$, $J_3 = 0.4$.

Figure 8(b) shows the corresponding extrapolated CCM LSUB∞ results for the GS energy per spin E/N of the spiral and striped states, as functions of the parameter J_3, for the same fixed values of J_2 shown in Fig. 8(a). The first-order transition between the spiral and striped states can clearly be seen to occur close to, but not precisely at, the corresponding maxima in the energy curves.

As before, the actual phase boundary is most clearly seen from our similarly extrapolated CCM LSUB∞ results for the magnetic order parameter M shown in Fig. 9. For all values of $J_2 \gtrsim 0.66$, there is a clear and sharp minimum in M at the phase-transition point in the parameter J_3 where the striped and spiral phases meet. When $J_2 \approx 0.66$, the two curves meet at $M = 0$. For this value of J_2, the magnetic order parameter M for the spiral state is very small (and positive) for all values of J_3, and as J_2 is decreased further, the spiral state rapidly disappears altogether for $J_2 \lesssim 0.635$. In the very narrow regime $0.635 \lesssim J_2 \lesssim 0.66$, we see from Fig. 9 that there appears to be an intrusion of the intermediate (quantum paramagnetic) phase, as shown in Fig. 2 by the appearance of both (cyan) open triangle ($\triangle$) and (orange) open circle ($\bigcirc$) symbols at the striped-spiral phase boundary at the two values $J_2 = 0.64, 0.65$. It seems almost sure, however, that this effect arises from our extrapolations, and is an indication of the (small) errors inherent in them. Our best estimate from the results shown in Fig. 9 is thus that the second tricritical QCP, where the spiral, striped, and quantum paramagnetic phases meet, occurs at $(J_2^{c_2}, J_3^{c_2}) = (0.65 \pm 0.02, 0.55 \pm 0.01)$.

We also note from Fig. 9 that when $0.635 \lesssim J_2 \lesssim 0.77$ and $J_3 > 0$, the magnetic order parameter M of the striped state becomes zero at a lower critical value of J_3. For the special case $J_3 = 0$ investigated earlier,[14] the spiral state is actually unstable since the Néel-II state was seen to have lower energy for all values of J_2 in the range investigated, namely, $J_2 \leqslant 1$, where solutions for the spiral state could be found. From continuity we expect the Néel-II state to remain the stable GS phase for small enough values of J_3 below some critical value for each fixed value of J_2, above which value the spiral phase becomes the stable GS phase. Thus, we are led to expect that there might exist a third tricritical QCP at $(J_2^{c_3}, J_3^{c_3})$ between the spiral, quantum paramagnetic, and Néel-II GS phases. We examine this further in Sec. V D.

D. Spiral versus Néel-II phases

In Fig. 10, we show results for the GS energy per spin E/N of both the spiral and Néel-II states as functions of the parameter J_3, for various fixed values of the parameter J_2 in the range $0.7 \leqslant J_2 \leqslant 1.0$. Although the energy differences are small for each fixed value of J_2, the results at each LSUBm level, as well as the extrapolated results, clearly show an energy crossing point. These energy crossing points are thus our first estimates of the phase-boundary points between the spiral and Néel-II states.

Since the energy differences of the spiral and Néel-II states are relatively small, we have found it preferable to use the extrapolation scheme of Eq. (8) in this case, and to employ the same data set with $m = \{4,6,8\}$ for both (Néel-II and spiral) phases, even though results with $m = 10$ are more readily available for the Néel-II state. We have, however, demonstrated that the results so obtained are robust and

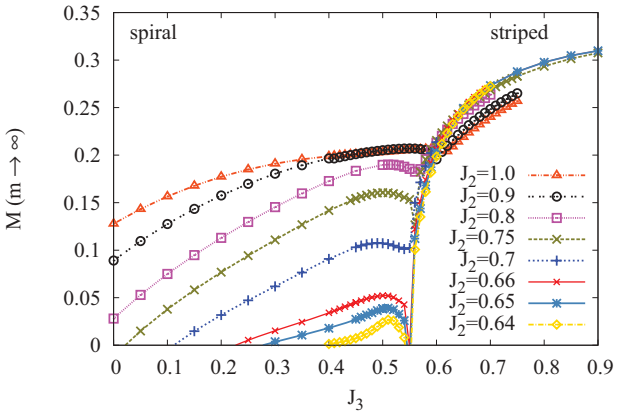

FIG. 9. (Color online) Extrapolated CCM LSUB∞ results for the GS magnetic order parameter M as a function of J_3, for various fixed values of J_2 in the range $0.64 \leqslant J_2 \leqslant 1.0$, for the spiral and the striped states. The extrapolated LSUBm ($m \to \infty$) results are based on the scheme of Eq. (9) and the calculated results with $m = \{4,6,8\}$. For the spiral state, the results use the pitch angle $\phi = \phi_{\mathrm{LSUB}m}$ that minimizes the energy $E = E_{\mathrm{LSUB}m}(\phi)$.

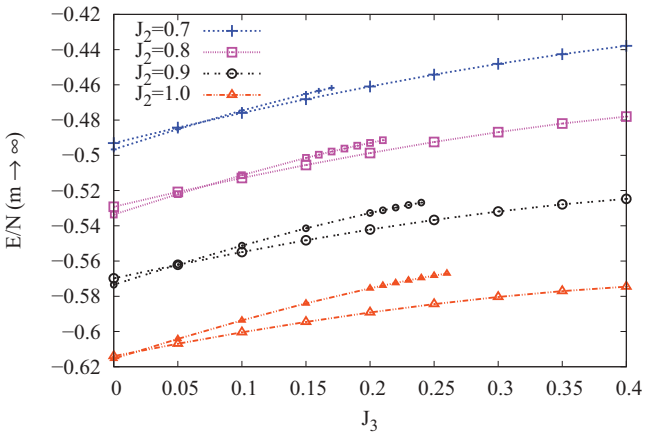

FIG. 10. (Color online) Extrapolated CCM LSUB∞ results for the GS energy per spin E/N as a function of J_3, for various fixed values of J_2 in the range $0.7 \leqslant J_2 \leqslant 1.0$, for the Néel-II and the spiral states. The extrapolated LSUBm ($m \to \infty$) results are based on the scheme of Eq. (8), and the calculated results with $m = \{4,6,8\}$ in both cases. Results for the spiral state use the pitch angle $\phi = \phi_{\mathrm{LSUB}m}$ that minimizes the energy $E = E_{\mathrm{LSUB}m}(\phi)$. Curves with small symbols attached refer to the Néel-II state, whereas those with large symbols refer to the spiral state.

reliable by making further checks in some limited test cases using the extrapolation scheme of Eq. (6) fitted to the results $m = \{4,6,8,10\}$ or the extrapolation scheme of Eq. (8) fitted to the results $m = \{6,8,10\}$, for example.

Real CCM LSUBm solutions based on the Néel-II state as model state cease to exist, for a fixed value of J_2, above some termination value in the parameter J_3 that itself depends on the truncation index m, just as we have indicated above for other phases. These LSUB8 terminations are what cause our extrapolations for the Néel-II state to be shown only up to certain values of J_3 for each curve shown in Fig. 10. In each case, the LSUBm solution with a finite value of m extends further into the region where the Néel-II solution actually ceases to exist (i.e., to after the energy crossing point with the spiral phase). Presumably, in the $m \to \infty$ limit, the LSUBm termination points for the Néel-II phase would coincide with the phase boundary with the spiral phase. Simple heuristic extrapolations based on the results with $m = \{4,6,8\}$ agree well with the energy crossing points, and are hence entirely consistent with this hypothesis.

We note from Fig. 10 that as the parameter J_2 is decreased towards the lower limiting value $J_2 \approx 0.635$, below which the spiral state ceases to exist, the energy curves for the Néel-II and spiral phases lie increasingly close to one another, and hence the crossing point becomes increasingly difficult to determine. Accordingly, we expect that a better indicator of the phase boundary might be obtained from a comparison of the magnetic order parameters of the two states, as now shown in Fig. 11.

For values of $J_2 \gtrsim 0.69$, the curves for the magnetic order parameters M of the Néel-II and spiral phases cross in the physical regime (i.e., at a positive value of M). These crossing

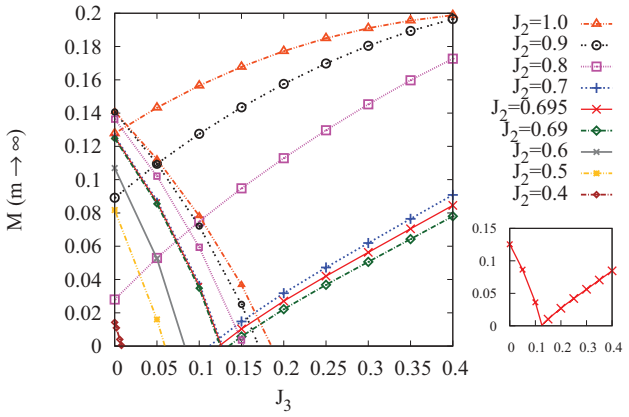

FIG. 11. (Color online) Extrapolated CCM LSUB∞ results for the GS magnetic order parameter M as a function of J_3, for various fixed values of J_2 in the range $0.4 \leqslant J_3 \leqslant 1.0$, for the Néel-II and the spiral states. The extrapolated LSUBm ($m \to \infty$) results are based on the scheme of Eq. (9), and the calculated results with $m = \{4,6,8\}$ for both the Néel-II and spiral phases for values $J_2 = 0.69,0.695,0.7,0.8,0.9,1.0$; and with $m = \{6,8,10\}$ for the Néel-II phase for values $J_2 = 0.4,0.5,0.6$. For the spiral state, the results use the pitch angle $\phi = \phi_{\text{LSUB}m}$ that minimizes the energy $E = E_{\text{LSUB}m}(\phi)$. Curves with small symbols attached (left curves) refer to the Néel-II state, whereas those with large symbols (right curves) refer to the spiral state.

points are our best estimates for the corresponding points on the boundary between the two phases, and these are shown in the phase diagram of Fig. 2 by (magenta) times ($\times$) symbols. For $J_2 \gtrsim 0.8$, these values are in excellent quantitative agreement with the corresponding energy crossing points from Fig. 10. For smaller values of J_2, down to $J_2 \approx 0.635$, below which the spiral state ceases to exist for any value of J_3, the energy crossing points become increasingly difficult to estimate accurately, as discussed above, and generally lie slightly below the much more accurate values obtained from Fig. 11, although still in good qualitative agreement with them.

Our best estimate for the position of the third tricritical QCP $[(J_2^{c_3}, J_3^{c_3}) = (0.69 \pm 0.01, 0.12 \pm 0.02)]$, which marks the point where the spiral and Néel-II phases meet the QP phase, comes from curves such as those shown in Fig. 11. For values $J_2 < J_2^{c_3} \approx 0.69$, we use the corresponding values of J_3 at which the magnetic order parameter $M \to 0$ for the Néel-II phase, as shown in Fig. 11, to find the phase boundary between the Néel-II and QP phases. The corresponding points are shown in the phase diagram of Fig. 2 by (blue) plus (+) symbols.

E. Quantum paramagnetic (PVBC?) phase(s)

So far, we have seen that in the parameter-space window $J_2, J_3 \in [0,1]$, the spin-1/2 J_1-J_2-J_3 HAFM on the honeycomb lattice with $J_1 \equiv 1$ has regions of five different GS phases. Four of these (viz., the Néel, striped, Néel-II, and spiral phases) are quasiclassical in nature, and they almost completely surround the fifth QP phase, as shown in Fig. 2, with each of them sharing a boundary with the (almost) enclosed region of the QP phase. (Indeed, it seems likely that if the diagram were extended slightly to negative values of J_3, the QP region would be seen to be entirely enclosed.) In the window $J_2, J_3 \in [0,1]$, there are three tricritical QCPs (and it seems likely that a fourth, which marks the meeting of the Néel, Néel-II, and QP phases, will occur just outside the window).

From our current results discussed here, the question still remains open, however, as to the exact nature of the QP phase. What we know from previous CCM work[8,14] is that the QP phase appears to have PVBC ordering at least at four points along its boundary. These include the two points marked with the larger (red) times ($\times$) symbols in Fig. 2 along its boundary with the Néel state where it crosses both the $J_3 = 0$ axis and the $J_3 = J_2$ line, the point marked with the larger (green) plus (+) symbol along its boundary with the striped state where it crosses the $J_3 = J_2$ line, and the point marked with the larger (blue) plus (+) symbol along its boundary with the Néel-II state where it crosses the $J_3 = 0$ axis.

Those points were identified as lying on a phase boundary with the PVBC state by calculating, within the same CCM LSUBm approximations as used to calculate the phase-transition points that marked the vanishing of the magnetic order parameter M in each case (i.e., for the Néel, striped, and Néel-II phases, respectively), the susceptibility of the respective phases against the formation of PVBC order. We showed, within the accuracy of our results, that each of the above four points where the respective magnetic order parameter of each quasiclassical phase goes to zero coincide

with the points at which the corresponding susceptibility of the state to PVBC order becomes infinite.

VI. SUMMARY AND DISCUSSION

We have studied the spin-1/2 HAFM on the honeycomb lattice with NN, NNN, and NNNN exchange interactions, namely, the so-called J_1-J_2-J_3 model described by the Hamiltonian of Eq. (1), in the case where all the bonds are antiferromagnetic in nature (i.e., $J_n > 0, n = 1,2,3$). We have set $J_1 \equiv 1$ to set the overall energy scale, and we have restricted attention here to the window $J_2, J_3 \in [0,1]$ for the remaining parameters.

Whereas in the classical model the only three phases present in the $J_2, J_3 \in [0,1]$ window (viz., the Néel, striped, and spiral phases) meet at a single tricritical point at $(J_2^{c,\mathrm{cl}}, J_3^{c,\mathrm{cl}}) = (0.5,0.5)$, there are now three tricritical QCPs in the same window for the $s = \frac{1}{2}$ model. The classical tricritical point separates into two tricritical QCPs at $(J_2^{c_1}, J_3^{c_1}) = (0.51 \pm 0.01, 0.69 \pm 0.01)$ between the Néel, striped, and QP phases, and at $(J_2^{c_2}, J_3^{c_2}) = (0.65 \pm 0.02, 0.55 \pm 0.01)$ between the striped, spiral, and QP phases. A third tricritical QCP at $(J_2^{c_3}, J_3^{c_3}) = (0.69 \pm 0.01, 0.12 \pm 0.02)$, is identified for the spin-1/2 model between the spiral, Néel-II, and QP phases.

In overall terms, our results for the phase diagram are in good agreement with other very recent analyses of this model. These include studies using a combination of various exact diagonalization (ED) and self-consistent cluster mean-field (SCCMF) techniques,[9,10] an unbiased pseudofermion functional renormalization group (PFFRG) method,[7] series expansion (SE) techniques,[11] and an entangled-plaquette variational (EPV) ansatz.[12] It is clear that the spin-1/2 J_1-J_2-J_3 HAFM on the honeycomb lattice is a challenging model, but one in which there seems now to be a growing consensus on its overall phase structure. There is very good agreement over the regions in which the Néel and striped phases exist, and we believe our own CCM results now give perhaps the best quantitative results in these cases for the positions of the phase boundaries and the positions of the two tricritical QCPs at $(J_2^{c_1}, J_3^{c_1})$ and $(J_2^{c_2}, J_3^{c_2})$.

An uncertainty remains over the precise extent of the phase with spiral order, and whether or not there is a Néel-II phase along the $J_3 = 0$ line for values of J_2 beyond the point where the QP phase disappears, and hence also for small positive values of J_3 up to the point where spiral order sets in. The other main uncertainty is the nature of the QP phase itself. We have argued here that over at least some widely separated points on the boundaries with the Néel, striped, and Néel-II phases, the QP phase has PVBC order. Two quite separate ED calculations[9,10] also give clear evidence that much of the QP phase has PVBC order, although the latter calculations[10] are only done along the $J_3 = 0$ line.

By contrast, the EPV calculations[12] along the $J_3 = 0$ line seem to favor a disordered (QSL) phase, while spin-wave calculations[3] favor the staggered dimer valence-bond crystalline (SDVBC) order of the lattice nematic state along the same line in the QP regime. The PFFRG study,[7] also done over the entire $J_2, J_3 \in [0,1]$ window, finds evidence too that a large part of the QP regime has strong SDVBC order, while the part with smaller values of J_2 has only weak PVBC order. On the other hand, the SE study[11] finds that SDVBC order is not favored, at least for low values of J_3.

We should note, however, that the SE study is in broad disagreement with most other studies along the $J_3 = 0$ line, in that it finds no evidence at all for a magnetically disordered phase there, but instead finds that the Néel phase first gives way to the second classical spiral phase, and then later to the spiral phase considered here, as J_2 is increased. On the other hand, the SE results are consistent with the finding from the ED + SCCMF analysis[9] that at least for some parameter ranges, the SDVBC state might be very difficult to distinguish from magnetically ordered states such as our S state.

Finally, we note that the ED + SCCMF study also presents evidence for the Néel to PVBC transition being a strong candidate for a deconfined transition, just as we have found in our earlier CCM studies of the model along the $J_3 = J_2$ line[8] and along the $J_3 = 0$ line.[14] Clearly, this model still has open questions, but we believe that the CCM results presented here have furthered our understanding of it.

ACKNOWLEDGMENTS

We thank J. Richter for fruitful discussions. We are also grateful to J. Schulenburg for his assistance in the updating and maintenance of the CCM computer code. We thank the University of Minnesota Supercomputing Institute for the grant of supercomputing facilities.

[1] E. Rastelli, A. Tassi, and L. Reatto, Physica B & C (Amsterdam) **97**, 1 (1979).
[2] J. B. Fouet, P. Sindzingre, and C. Lhuillier, Eur. Phys. J. B **20**, 241 (2001).
[3] A. Mulder, R. Ganesh, L. Capriotti, and A. Paramekanti, Phys. Rev. B **81**, 214419 (2010).
[4] D. C. Cabra, C. A. Lamas, and H. D. Rosales, Phys. Rev. B **83**, 094506 (2011).
[5] R. Ganesh, D. N. Sheng, Y.-J. Kim, and A. Paramekanti, Phys. Rev. B **83**, 144414 (2011).
[6] B. K. Clark, D. A. Abanin, and S. L. Sondhi, Phys. Rev. Lett. **107**, 087204 (2011).
[7] J. Reuther, D. A. Abanin, and R. Thomale, Phys. Rev. B **84**, 014417 (2011).
[8] D. J. J. Farnell, R. F. Bishop, P. H. Y. Li, J. Richter, and C. E. Campbell, Phys. Rev. B **84**, 012403 (2011).
[9] A. F. Albuquerque, D. Schwandt, B. Hetényi, S. Capponi, M. Mambrini, and A. M. Läuchli, Phys. Rev. B **84**, 024406 (2011).
[10] H. Mosadeq, F. Shahbazi, and S. A. Jafari, J. Phys.: Condens. Matter **23**, 226006 (2011).
[11] J. Oitmaa and R. R. P. Singh, Phys. Rev. B **84**, 094424 (2011).
[12] F. Mezzacapo and M. Boninsegni, Phys. Rev. B **85**, 060402(R) (2012).

[13]P. H. Y. Li, R. F. Bishop, D. J. J. Farnell, J. Richter, and C. E. Campbell, Phys. Rev. B **85**, 085115 (2012).
[14]R. F. Bishop, P. H. Y. Li, D. J. J. Farnell, and C. E. Campbell, J. Phys.: Condens. Matter **24**, 236002 (2012).
[15]R. F. Bishop and P. H. Y. Li, Phys. Rev. B **85**, 155135 (2012).
[16]A. Kitaev, Ann. Phys. (NY) **321**, 2 (2006); G. Baskaran, S. Mandal, and R. Shankar, Phys. Rev. Lett. **98**, 247201 (2007); J. Chaloupka, G. Jackeli, and G. Khaliullin, *ibid*. **105**, 027204 (2010).
[17]A. H. Castro Neto, F. Guinea, N. M. R. Peres, K. S. Novoselov, and A. K. Geim, Rev. Mod. Phys. **81**, 109 (2009).
[18]Z. Y. Meng, T. C. Lang, S. Wessel, F. F. Assaad, and A. Muramatsu, Nature (London) **464**, 847 (2010).
[19]H. Y. Yang and K. P. Schmidt, Europhys. Lett. **94**, 17004 (2011).
[20]A. Vaezi and X. G. Wen, arXiv:1010.5744.
[21]A. Vaezi, M. Mashkoori, and M. Hosseini, Phys. Rev. B **85**, 195126 (2012).
[22]S. Okubo, F. Elmasry, W. Zhang, M. Fujisawa, T. Sakurai, H. Ohta, M. Azuma, O. A. Sumirnova, and N. Kumada, J. Phys.: Conf. Series **200**, 022042 (2010).
[23]Y. Miura, R. Hiari, Y. Kobayashi, and M. Sato, J. Phys. Soc. Jpn. **75**, 084707 (2006).
[24]V. Kataev, A. Möller, U. Löw, W. Jung, N. Schittner, M. Kriener, and A. Freimuth, J. Magn. Magn. Mater. **290/291**, 310 (2005).
[25]L. P. Regnault and J. Rossat-Mignod, in *Phase Transitions in Quasi-Two-Dimensional Planar Magnets*, edited by L. J. De Jongh (Kluwer Academic, Dordrecht, 1990), p. 271.
[26]A. A. Tsirlin, O. Janson, and H. Rosner, Phys. Rev. B **82**, 144416 (2010).
[27]C. Zeng, D. J. J. Farnell, and R. F. Bishop, J. Stat. Phys. **90**, 327 (1998).
[28]R. Darradi, J. Richter, and D. J. J. Farnell, Phys. Rev. B **72**, 104425 (2005).
[29]D. Schmalfuß, R. Darradi, J. Richter, J. Schulenburg, and D. Ihle, Phys. Rev. Lett. **97**, 157201 (2006).
[30]R. F. Bishop, P. H. Y. Li, R. Darradi, J. Schulenburg, and J. Richter, Phys. Rev. B **78**, 054412 (2008).
[31]R. F. Bishop, P. H. Y. Li, R. Darradi, and J. Richter, J. Phys.: Condens. Matter **20**, 255251 (2008).
[32]R. Darradi, O. Derzhko, R. Zinke, J. Schulenburg, S. E. Krüger, and J. Richter, Phys. Rev. B **78**, 214415 (2008).
[33]R. F. Bishop, P. H. Y. Li, D. J. J. Farnell, and C. E. Campbell, Phys. Rev. B **79**, 174405 (2009).
[34]J. Reuther, P. Wölfle, R. Darradi, W. Brenig, M. Arlego, and J. Richter, Phys. Rev. B **83**, 064416 (2011).
[35]R. F. Bishop, P. H. Y. Li, D. J. J. Farnell, J. Richter, and C. E. Campbell, Phys. Rev. B **85**, 205122 (2012).
[36]H. J. Schulz, T. A. L. Ziman, and D. Poilblanc, J. Phys. I **6**, 675 (1996).
[37]J. Richter and J. Schulenberg, Eur. Phys. J. B **73**, 117 (2010).
[38]We use the program package CCCM of D. J. J. Farnell and J. Schulenburg, see http://www-e.uni-magdeburg.de/jschulen/ccm/index.html